SLC4A10 mutation causes a neurological disorder associated with impaired GABAergic transmission

James Fasham,[1,2,†] Antje K. Huebner,[3,†] Lutz Liebmann,[3,†] Reham Khalaf-Nazzal,[4,†] Reza Maroofian,[5] Nderim Kryeziu,[3] Saskia B. Wortmann,[6,7,8] Joseph S. Leslie,[1] Nishanka Ubeyratna,[1] Grazia M. S. Mancini,[9] Marjon van Slegtenhorst,[9] Martina Wilke,[9] Tobias B. Haack,[10] Hanan Shamseldin,[11] Joseph G. Gleeson,[12,13] Mohamed Almuhaizea,[14] Imad Dweikat,[4] Bassam Abu-Libdeh,[15] Muhannad Daana,[16] Maha S. Zaki,[17] Matthew N. Wakeling,[1] Lucy McGavin,[18] Peter D. Turnpenny,[1,2] Fowzan S. Alkuraya,[11] Henry Houlden,[5] Peter Schlattmann,[19] Kai Kaila,[20,21] Andrew H. Crosby,[1] Emma L. Baple[1,2] and Christian A. Hübner[3,22]

[†]**These authors contributed equally to this work.**

Abstract

SLC4A10 is a plasma-membrane bound transporter which utilizes the Na^+ gradient to drive cellular HCO_3^- uptake, thus mediating acid extrusion. In the mammalian brain, *SLC4A10* is expressed in principal neurons and interneurons, as well as in epithelial cells of the choroid plexus, the organ regulating the production of cerebrospinal fluid.

Using next generation sequencing on samples from five unrelated families encompassing ten affected individuals, we show that biallelic *SLC4A10* loss-of-function variants cause a clinically recognizable neurodevelopmental disorder in humans. The cardinal clinical features of the condition include hypotonia in infancy, delayed psychomotor development across all domains and typically severe intellectual impairment. Affected individuals commonly display traits associated with autistic spectrum disorders including anxiety, hyperactivity and stereotyped movements. In two cases isolated episodes of seizures were reported in the first few years of life, and a further affected child displayed bitemporal epileptogenic discharges on EEG without overt clinical seizures. While occipitofrontal circumference was reported to be normal at birth, progressive postnatal microcephaly evolved in 7 out of 10 affected individuals. Neuroradiological features included a relative preservation of brain volume compared to occipitofrontal circumference, characteristic narrow sometimes 'slit-like' lateral ventricles and corpus callosum abnormalities.

Slc4a10^{-/-} mice, deficient for SLC4A10, also display small lateral brain ventricles and mild behavioral abnormalities including delayed habituation and alterations in the 2-object novel object recognition task. Collapsed brain ventricles in both *Slc4a10^{-/-}* mice and affected individuals suggests an important role of SLC4A10 in the production of the cerebrospinal fluid. However, it is notable that despite diverse roles of the cerebrospinal fluid in the developing and adult brain, the cortex of *Slc4a10^{-/-}* mice appears grossly intact.

Co-staining with synaptic markers revealed that in neurons, SLC4A10 localizes to inhibitory, but not excitatory, presynapses. These findings are supported by our functional studies which show the release of the inhibitory neurotransmitter GABA is compromised in *Slc4a10^{-/-}* mice, while the release of the excitatory neurotransmitter glutamate is preserved. Manipulation of intracellular pH partially rescues GABA release.

Together our studies define a novel characteristic neurodevelopmental disorder associated with biallelic pathogenic variants in *SLC4A10* and highlight the importance of further analyses of the consequences of SLC4A10 loss-of-function for brain development, synaptic transmission and network properties.

Author affiliations:

1 RILD Wellcome Wolfson Centre, University of Exeter Medical School, Royal Devon & Exeter NHS Foundation Trust, Exeter, EX2 5DW, UK

2 Peninsula Clinical Genetics Service, Royal Devon & Exeter Hospital, Exeter, EX2 5DW, UK

3 Institute of Human Genetics, Jena University Hospital, Friedrich Schiller Universität, Am Klinikum 1, 07747, Jena, Germany

4 Faculty of Medicine, Arab American University of Palestine, Jenin, Palestine

5 Molecular and Clinical Sciences Institute, St. George's University of London, Cranmer Terrace, London, SW17 0RE, UK

6 University Children's Hospital, Salzburger Landeskliniken (SALK) and Paracelsus Medical University (PMU), 5020 Salzburg, Austria

7 Amalia Children's Hospital, Radboudumc, 6525 GA Nijmegen, The Netherlands

8 Institute of Human Genetics, Technische Universität München, 80333 Munich, Germany

9 Erasmus Medical Center, room Ee2077, Dr Molewaterplein 40. 3015 GD Rotterdam, The Netherlands

10 Institute of Medical Genetics and Applied Genomics, University of Tuebingen, 72076 Tübingen, Germany

11 Department of Translational Genomics, Center for Genomic Medicine, King Faisal Specialist Hospital and Research Center, Riyadh 11564, Saudi Arabia

12 Rady Children's Institute for Genomic Medicine, San Diego, CA 92123, USA

13 University of California, San Diego, La Jolla, CA 92093, USA

14 Department of Neuroscience, King Faisal Specialist Hospital and Research Center, Riyadh 11564, Saudi Arabia

15 Department of Pediatrics and Genetics, Makassed Hospital and Al-Quds University, East Jerusalem, Palestine

16 Arab Women's Union Hospital, Nablus, Palestine

17 Clinical Genetics Department, Human Genetics and Genome Research Division, National Research Centre, Dokki, Cairo 12622, Egypt

18 Department of Radiology, Derriford Hospital, Plymouth, PL6 8DH, UK

19 Institute for Medical Statistics, Computer Science and Data Science, Jena University Hospital, 07747 Jena, Germany

20 Molecular and Integrative Biosciences, University of Helsinki, 00014 Helsinki, Finland

21 Neuroscience Center, Helsinki Institute of Life Science, University of Helsinki, 00014 Helsinki, Finland

22 Center for Rare Diseases, Jena University Hospital, 07747 Jena, Germany

Correspondence to: Prof Andrew H. Crosby

1 RILD Wellcome Wolfson Centre, University of Exeter Medical School, Royal Devon & Exeter

2 NHS Foundation Trust, Barrack Rd, Exeter EX2 5DW, UK

3 E-mail: a.h.crosby@exeter.ac.uk

4

5 Correspondence may also be addressed to: Prof. Emma L. Baple

6 E-mail: E.Baple@exeter.ac.uk

7

8 Prof. Christian A. Hübner

9 Institute of Human Genetics, University Hospital Jena, Jena, 7747, Germany

10 E-mail: christian.huebner@med.uni-jena.de

11

18

Introduction

20 A large variety of molecules involved in neuronal signaling, including ligand- and voltage-gated
21 channels, show a remarkable sensitivity to changes in the intracellular and extracellular pH.[1-4] As
22 a rule, the excitability of neuronal networks is enhanced by alkalosis and suppressed by acidosis,[5-
23 7] which suggests a fundamental evolutionary role for pH as a neuromodulator during physiological
24 and pathophysiological conditions. Numerous studies have provided evidence for mechanisms that
25 control pH dynamics and actions in microdomains within[8-13] and outside[12] brain cells based on the
26 heterogeneous spatial patterns of expression of both pH-sensitive and pH-regulatory proteins,

including plasmalemmal Na^+/H^+ exchangers[14], HCO_3^- transporters[15,16] as well as intra- and extracellular carbonic anhydrase isoforms.[4]

In mammals, members of the SLC4[15] and SLC26[16] gene families have been identified as bicarbonate (HCO_3^-) transporters, many of which are associated with monogenic human diseases including distal renal tubular acidosis, hemolytic anemia, corneal dystrophy, glaucoma and cataracts,[15] as well as chondrodysplasia, chloride diarrhea, and hearing loss.[17] The SLC4 family includes Na^+-independent Cl^-/HCO_3^- exchangers, electrogenic and electroneutral Na^+-HCO_3^- cotransporters and Na^+-driven Cl^-/HCO_3^- exchangers that mediate HCO_3^- transport across the plasma membrane[15] (**Table S1**). SLC4A10 utilizes the transmembrane gradient of Na^+ to drive cellular net uptake of HCO_3^-, and thus mediates acid extrusion. Both cytoplasmic and membrane-bound carbonic anhydrases are involved in the supply of bicarbonate and may thus increase transport rates.[18] To which extent this is relevant for SLCA10 mediated transport is yet unclear. Some controversy exists as to whether it acts as an electroneutral Na^+-HCO_3^- cotransporter (NBCn2), or a Na^+-coupled Cl^-/HCO_3^- exchanger (NCBE) under physiological conditions.[19,20] The expression of *SLC4A10* is predominantly neuronal, but it is also expressed in choroid plexus epithelia[21,22] and in inner ear fibrocytes[23]. Mice deficient for SLC4A10 show a reduced brain ventricle size suggesting a role in transepithelial electrolyte transport and production of cerebrospinal fluid[22]. Although neuronal excitability was enhanced *in vitro*[24], the experimental seizure threshold was paradoxically increased *in vivo*[22] and spontaneous seizures were not observed.

In humans, heterozygous genomic deletions comprising all or part of *SLC4A10* have been linked with autistic spectrum disorder, with additional features such as impaired motor and language skills or epilepsy.[25-28] The causal relevance of these genomic alterations is, however, unclear, as the interpretation of these findings is complicated by contiguous gene deletion. Here, we provide clinical, genetic, functional and mouse-model evidence to determine that autosomal recessive SLC4A10 loss of function results in intellectual disability with striking radiological abnormalities of the lateral ventricles, closely mirroring findings in *Slc4a10* knockout (KO) mice. As SLC4A10 localizes to inhibitory presynapses and its disruption compromises γ-aminobutyric acid (GABA) release, we propose that alterations of the GABAergic system contribute to the pathomechanistic basis of this neurodevelopmental disorder.

1 Materials and methods

2 Clinical studies

3 All families were recruited with written informed consent according to international guidelines,
4 including the Declaration of Helsinki, and regional ethical approvals (Palestinian Health Research
5 Council PHRC/HC/518/19, Technische Universität München, Muenchen Exome Seq.: 5360/12 S,
6 KFSHRC RAC # 2121053, Erasmus MC METC 2012-387, IRB protocol number 150765).
7 Affected individuals were examined and investigated by local clinicians according to routine
8 clinical standards relevant to their clinical presentation.

9 Genetic studies

10 DNA and RNA were extracted from blood/buccal samples using standard techniques. In all five
11 families whole genome sequencing (WGS) (Family 1) or whole exome sequencing (WES)
12 (Families 2-5) was undertaken to identify the cause of disease. Family pedigrees illustrating the
13 relationships of affected and unaffected individuals in this study are shown in **Fig. 1**. Unless
14 otherwise specified, genomic variants were filtered based on call quality, predicted consequence,
15 segregation with the disease phenotype and allele frequency in population databases (variants with
16 a frequency of >0.1% and/or present in >1 homozygous individual in gnomAD v2.1.1, v3.1.1 or
17 in-house databases were excluded). Homozygous, compound heterozygous, X chromosome and
18 *de novo* (when trio sequencing undertaken) variants present in exons or within ±6 nucleotides in
19 the intron that remained after filtering, were assessed for clinical correlation with the affected
20 individual(s) phenotype.

21

22 In Family 1, WGS was performed (BGI, Hong Kong) on DNA from two affected individuals
23 (Family 1, II:1 and II:2). Reads were aligned (BWA-MEM v0.7.15), mate-pairs fixed, and
24 duplicates removed (Picard v2.7.1), InDel realignment/base quality recalibration (GATK v3.7.0),
25 single-nucleotide variant (SNV)/InDel detection (GATK HaplotypeCaller), annotation (Alamut
26 v1.11), and read depth ascertained using an in-house pipeline. This conforms to GATK best
27 practices. Copy number variants (CNVs) were detected using SavvyCNV.[29]

In Family 2, DNA from the proband (II:1) and both unaffected parents underwent trio WES (Illumina) at Technical University München/Helmholtz Institute Neuherberg using the SureSelect50Mbv5 capture, as previously described.[30,31] In Family 3, trio WES of a single affected individual (II:2) and both parents was undertaken as previously described (ID: 17-4393).[32] In Family 4 WES was performed on the two affected brothers at University of California San Diego (UCSD) using methods previously described,[33] with recessive variants within regions of homozygosity prioritized given the consanguineous nature of the family. In Family 5, trio WES was performed on both affected siblings and their two unaffected parents (four individuals in total) using Agilent SureSelect Target Enrichment Clinical Research Exome V2 (Agilent Technologies, Santa Clara, CA, USA). Sequencing (paired-end 150bp) was performed by the Illumina HiSeq 4000 platform (Illumina, San Diego, CA, USA, outsourced). Data were demultiplexed by Illumina Software CASAVA. Reads are mapped to the genome (build hg19/GRCh37) with the program BWA (reference: http://bio-bwa.sourceforge.net/). Variants were detected with the Genome Analysis Toolkit (reference: http://www.broadinstitute.org/gatk/). Variants were filtered with the Cartagenia/Alissa Interpret software package (Agilent technologies) on quality (read depth ≥10), frequency in databases (≥1% in 200 alleles in dbSNP, ESP6500, the 1000 Genome project or the ExAC database) and location (within an exon or first/last 10 bp of introns).

In Family 1 unique primers for droplet digital polymerase chain reaction (ddPCR) (QX200 AutoDG Droplet Digital PCR System - Bio Rad, CA, USA) were designed for confirmation and cosegregation of the exon 5-11 *SLC4A10* deletion [NM_001178015: c.417_1341del]. In addition to two primers within the deletion (within exons 5 and 10), probes included an exon 5' to the deletion (Exon 4), an exon 3' to the deletion (Exon 11) and a housekeeping gene control (*RPP30*). Primer sequences are provided (**Supplementary Fig. 1).**

In Family 3 reverse transcription PCR (RT-PCR), using standard techniques, was undertaken on lymphoblast cell lines derived from affected and controls individuals to confirm the transcriptional outcome of the *SLC4A10* NM_001178015:c.2863-2A>C variant. RNA was extracted using RNeasy kit (QIAGEN-Catalogue # 74104) as per the manufacturer's protocol. cDNA was generated from 1 µg of RNA via iScript Select cDNA Synthesis kit (Bio-rad). Primers that cover

exons 19-24 of *SLC4A10* transcript were used for RT-PCR to check for difference in splicing between affected and control lymphoblast.

In Families 2-4, dideoxy sequencing confirmation and cosegregation of single nucleotide *SLC4A10* variants was performed using standard techniques.

Cellular studies

Cloning

The human *SLC4A10* cDNA was cloned by PCR from a human cDNA library and subcloned into the pBI-CMV4 vector (Clon-tech #PT4443-5), a mammalian bidirectional expression vector designed to constitutively express a protein of interest and DsRed2, a human codon-optimized variant of the *Discosoma sp.* red fluorescent protein. Disease associated single nucleotide variants were inserted by site-directed mutagenesis and verified by sequencing.

Cell Culture

N2a cells were cultured at 37°C with Dulbecco's Eagle's Minimum Essential Medium (DMEM) (Gibco #31966-021) supplemented with fetal bovine serum to a final concentration of 10% and 1% penicillin/streptomycin (Gibco #15070063). N2a cells were transfected with Lipofectamine 3000 (Invitrogen #L3000008) according to the manufacturer's instructions.

For staining, cells were fixed with 4% PFA in PBS for 10 min and subsequently washed. Cells were stained with WGA coupled to Biotin (Biozol #B-1025) at a dilution of 1:500 and a polyclonal rabbit anti-SLC4A10 antibody (1:500)[22] at 4°C overnight. The secondary antibodies we used were a Streptavidin-Alexa Fluor 488 conjugate (1:1000, Invitrogen #S32354) and an Alexa Fluor 546-coupled goat anti-rabbit antibody (1:1000, Invitrogen). Transfection rates varied between 20 and 40% with no obvious effect of the genotype of the transfected construct. Analysis was done with a confocal microscope in the Airyscan mode (LSM 880, Zeiss). The plasma membrane region (PMR) was determined as the WGA-labelled cell rim.

Intracellular pH recordings

48h after transfection, the intracellular pH (pH_i) was measured using the ratiometric 2′,7′-Bis(2-carboxyethyl)-5(6)-carboxyfluorescein (BCECF, Molecular Probes) fluorescent dye. Cells were

washed with bicarbonate-buffered solution containing (in mM): 99 NaCl, 20 Na-gluconate, 5 KCl, 1 $MgSO_4$, 1.5 $CaCl_2$, 25 $NaHCO_3$ and 10 glucose. Coverslips were transferred to a heated perfusion chamber (Chamlide EC; Live Cell Instruments, 37 °C), which was mounted at an Axio Observer.Z1 microscope (Zeiss). An image was acquired for the RFP channel to identify transfected cells. Thereafter, BCECF-AM was added to a final concentration of 4 µM and incubated for 10 min. The cells were superfused with bicarbonate-buffered solution at a linear flow rate of 2.5 ml/s. Emitted light of 510-535 nm was recorded after alternating excitation at 495 nm and 440 nm every 10 s and captured through a 10x objective with a CCD-camera (AxioCam MRm; Zeiss). The steady state pH_i was recorded for 5 min. Then 5 µM EIPA was added to the perfusion buffer to block Na^+/H^+ exchange activity and the pH recorded for another 5 min. The superfusion was then switched to bicarbonate-buffered solution containing 5 µM EIPA and 20 mM sodium propionate instead of 20 mM Na^+-gluconate for 5 min. After the propionate pulse cells were superfused again with the former used bicarbonate-buffered solution supplemented with 5 µM EIPA. The cytoplasmic pH recovery was recorded during superfusion with 20 mM sodium propionate containing bicarbonate-buffered solution. For each coverslip more than 12 neighboring transfected and non-transfected cells were analyzed and data from different coverslips were averaged. At the end of each experiment, a calibration was done with buffers between pH 6.5 and 7.5 (in mM: 135 KCl, 20 N-methyl-D-glucamine, 4 $MgSO_4$, 10 glucose, 30 HEPES, 10 µM nigericin). A linear regression was calculated from the multipoint calibration curve, and F_{495}/F_{440} ratio was converted into pH_i values. Data regarding initial pH, amplitude of acidosis, recovery and pHi amplitude overshoot were obtained, with recovery from acidification being the primary outcome.

Mouse studies

The generation of $Slc4a10^{-/-}$ mice from a 129SvJ embryonic stem cell line was described previously.[22] All experiments were conducted according to the German Law on the Protection of Animals and the corresponding European Communities Council Directive of November 24, 1986 (86/609/EEC) and were approved by the Thüringer Landesamt für Lebensmittelsicherheit und Verbraucherschutz (Thuringia State Office for Food Safety and Consumer Protection) under the registration number 02-001/13. Mice were group-housed on a 12-h light-dark cycle and fed with food and water *ad libitum*. If not indicated otherwise, the experiments started when the animals

were 3 to 4 months old and weighed 25–35 g. Tests were performed during the light phase between 10:00 a.m. and 5:00 p.m.

The 2-object novel object recognition (NOR) task was used to evaluate recognition memory in rodents in 12-month-old wild-type and knockout mice of both sexes. During habituation, the animals were allowed to explore an open field arena on two days with one day interval in between. One week after habituation, the animals were again exposed to the familiar arena but with two identical glass bottles with a blue cap placed at an equal distance. Four hours later, the mice were placed in the arena, after one glass bottle was replaced by a tower of yellow and green Lego bricks of the same height. Mice were recorded with a CCD camera (Panasonic) for ten minutes. The time spent exploring each object, the number of visits and the exploring time per visit were analyzed off-line with Microsoft Windows Movie Maker. The primary outcome was the difference score (time exploring novel object - time exploring familiar object) with the discrimination ratio (time exploring novel object / total time spent with both objects) also calculated.

Histology and immunohistochemistry

Hematoxylin and eosin (HE) staining followed standard protocols (Carl Roth, Germany). For immunofluorescence, brains of 2-to-3-month-old wild type mice were prepared and fixed as described previously.[8] Free-floating cryosections (50 µm) were stained with a polyclonal rabbit anti-NeuN antibody (1:1000, Abcam, ab104225) or polyclonal rabbit anti-SLC4A10 antibody.[22] For co-staining, the following primary antibodies were used: polyclonal guinea pig anti-vesicular GABA transporter (VGAT, 1:250, Synaptic Systems), polyclonal guinea pig anti-vesicular glutamate transporter 1 (VGLUT1, 1:500, Synaptic Systems). Alexa Fluor 488- and 546-coupled goat anti-rabbit and goat anti-guinea pig antibodies were used as secondary antibodies (1:1000, Invitrogen). Cell nuclei were stained by 4,6-diamidino-2-phenylindole (DAPI) (1 µg/ml, Sigma-Aldrich). Analysis was performed with a confocal microscope in the Airyscan mode (LSM 880, Zeiss). To quantify the degree of co-localization, planes were selected with an optimized signal-to-noise ratio using the range indicator and adjusting it to the linear, non-saturated range. Images were taken randomly from the hippocampal CA1 region (stratum radiatum or stratum pyramidale 225 x 225 µm) of four different wild-type brains. The relative area of colocalization was analyzed according to the Costes method.[34] Pearson coefficient was calculated as a measure of co-localization for each image using the colocalization module of ZEN (Release 4.8.2).

Slice preparation for electrophysiological recordings

Mice between two and three months of age were decapitated and the brain was removed from the skull and chilled (at ~4°C) in artificial cerebrospinal fluid (aCSF) containing (in mmol/L): 120 NaCl, 3 KCl, 5 $MgSO_4$, 1.25 NaH_2PO_4, 0.2 $CaCl_2$, 10 d-glucose, and 25 $NaHCO_3$, gassed with 95% O_2-5% CO_2. Horizontal brain slices (350 μm) including the hippocampus were prepared with a vibroslicer (Leica VT 1200S). Slices were stored at room temperature for at least 1h before use in recording aCSF containing (in mmol/L): 120 NaCl, 3 KCl, 1.3 $MgSO_4$, 1.25 NaH_2PO_4, 2.5 $CaCl_2$, 10 d-glucose, and 25 $NaHCO_3$, gassed with 95% O_2-5% CO_2, as described previously.[35]

Patch clamp recordings

One slice at a time was placed in a recording chamber mounted on an upright microscope (Axio Examiner.A1; Zeiss) with differential interference contrast, ×40 water-immersion objective, and ×10 ocular to identify cells. The slices were continuously perfused with aCSF (flow rate 2–3 ml/min, room temperature, pH 7.3) consisting of (in mM): 120 NaCl, 3 KCl, 1.3 $MgCl_2$, 2.5 $CaCl_2$, 25 $NaHCO_3$, 1.25 KH_2PO_4, and 10 d-glucose.

For whole-cell recordings patch pipettes with an impedance of ~3–4 MΩ were pulled from borosilicate glass (OD 1.5 mm; Science Products) with a micropipette puller (P-97, Sutter Instrument) and filled with intracellular solutions for miniature excitatory postsynaptic currents (mEPSC) or miniature inhibitory postsynaptic currents (mIPSC) recordings, respectively.

Pyramidal neurons of the CA1 and CA3 were selected for recording if they displayed a pyramidal-shaped cell body. Patched cells were voltage clamped. Only cells with a resting membrane potential below −55 mV and an access resistance <15 MΩ were included. Therefore, it was not necessary to compensate for the series resistance. Voltages were corrected for liquid junction potentials or series resistance. Signals were recorded using a patch-clamp amplifier (MultiClamp 700B; Axon Instruments). Responses were filtered at 5 kHz and digitized at 20 kHz (Digidata 1440A; Axon Instruments). All data were acquired, stored, and analyzed on a PC using pClamp 10 (Axon Instruments).

mEPSCs and mIPSCs were recorded at a holding potential of -70 mV for at least 5 min in aCSF. mEPSCs were isolated by adding tetrodotoxin (0.5 μM, Tocris Bioscience) to block action potential-induced glutamate release and bicuculline methiodide (20 μm, Biomol) to block $GABA_A$

1 responses. dl-APV (30 μM) was added to suppress NMDA currents. The pipette solution contained

2 the following (in mM): 120 CsMeSO$_4$, 17.5 CsCl, 10 HEPES, 5 BAPTA, 2 Mg-ATP, 0.5 Na-GTP,

3 10 QX-314 [N-(2,6-dimethylphenylcarbamoylmethyl) triethylammonium bromide], pH 7.3,

4 adjusted with CsOH.

5 Recordings of mIPSCs were performed using a CsCl-based intracellular solution (in mM): 122

6 CsCl, 8 NaCl, 0.2 MgCl$_2$, 10 HEPES, 2 EGTA, 2 Mg-ATP, 0.5 Na-GTP, 10 QX-314 [N-(2,6-

7 dimethylphenylcarbamoylmethyl)triethylammonium bromide], pH adjusted to 7.3 with CsOH. dl-

8 APV (30 μM), CNQX (10 μM) and tetrodotoxin (0.5 μM) were added to the perfusate. Recordings

9 of sIPSCs were performed in the absence of tetrodotoxin.

10 In a subset of mIPSC experiments, 20 mM NaCl was substituted by the weak base trimethylamine

11 chloride (TriMA; Sigma-Aldrich) to raise pH$_i$. In another subset of mIPSC experiments, 20 mM

12 NaCl was substituted by the weak acid sodium propionate (Sigma-Aldrich) to lower pH$_i$. After a

13 baseline recording of 5 min, the regular aCSF was replaced by aCSF with either TriMA or sodium

14 propionate, and mIPSCs were recorded for further 5 min.

15 For mIPSC recordings in bicarbonate-free extracellular solution we used (in mM): 130 NaCl, 3

16 KCl, 1.3 MgSO$_4$, 1.25 NaH$_2$PO$_4$, 2.5 CaCl$_2$, 10 D-glucose, 10 HEPES, gassed with O$_2$, pH 7.3

17 with NaOH.

18 The following parameters of mEPSCs and mIPSCs/sIPSCs were determined: frequency, peak

19 amplitude, time constant of decay (τ_{decay}), half-width, and electrical charge transfer, with analysis

20 of frequency the primary outcome measure. Data analysis was performed off-line with the

21 detection threshold levels set to 5 pA for mEPSCs and mIPSCs because of the peak-to-peak noise

22 determined under AMPA/NMDA receptor and GABA$_A$ receptor blockade.

Statistical analysis

24 Data are presented as mean +/- standard error of the mean (SEM).

25 To address potential issues with statistical analysis of the data associated with small sample sizes,

26 the distribution of the test statistics and corresponding p-values were obtained using the bootstrap

27 method (1000 replicates were applied as suggested in Dwivedi *et al.*).[36]

1 Comparison of two statistically independent experimental groups was performed with the two-

2 tailed t-test. If data were dependent, the paired t-test was used. In experiments that included more

3 than 2 groups, differences were tested by an F-test.

4 For correlated, replicated data we used a GEE model using normal errors identity link and

5 independent working correlation matrix. Calculations were performed in R and RStudio using the

6 package gee for the GEE model.[37-39]

7

Data availability

9 Full WGS and WES sequencing data are not available due to reasons of confidentiality;

10 anonymized variant data will be made available on reasonable request. The authors declare that all

11 other data are contained within the manuscript and supplemental materials. *SLC4A10* variants have

12 been deposited in ClinVar with submission number SUB11166749.

13

Results

Genetic analysis

16 We initially investigated the cause of disease in two male Palestinian siblings (aged 7 and 8 years)

17 affected by a syndromic form of severe intellectual disability, behaviors associated with autistic

18 spectrum disorder, slit ventricles and subtle craniofacial dysmorphism (Family 1). The younger

19 child was microcephalic, with an occipitofrontal circumference (OFC) of 3.4 standard deviation

20 scores below the mean (-3.4 SDS), whereas his older brother had an OFC of -2.3 SDS. To define

21 the genetic cause of disease WGS was performed on DNA from both affected children (Family 1,

22 II:1 and II:2). Filtering of WGS data using standard metrics described above identified a single

23 standout candidate variant, a shared, homozygous out-of-frame deletion of exons 5-11 of *SLC4A10*

24 [Chr2(GRCh38):g.161846109-161895992del;   NM_001178015:   c.417_1341del

25 p.(Trp140Argfs*39)] clearly visible on genome sequencing (**Supplementary Fig. 1**) and predicted

26 to result in nonsense-mediated decay (NMD) and absence of the SLC4A10 protein. The variant

1 was confirmed using ddPCR as an orthologous method and found to cosegregate as expected for

2 an autosomal recessive disorder (**Supplementary Fig. 2**).

3 Through collaborative studies (via GeneMatcher) we then identified eight additional affected

4 individuals from four unrelated families (**Fig. 1**), in whom WES identified biallelic rare predicted

5 loss-of-function *SLC4A10* variants (See **Fig. 1, Table 1, Supplemental case reports,**

6 **Supplementary Table 2** and **Supplementary Table 3** for family pedigrees, clinical details,

7 comprehensive case reports, *SLC4A10* variants and WGS/WES variant lists respectively). These

8 individuals (aged 4-17 years) presented with clinical features overlapping those of the Palestinian

9 children. In Family 2 trio WES (Individual II:1) identified a homozygous nonsense variant in exon

10 18/27 [Chr2(GRCh38):g.161949151C>T; NM_001178015:c.2269C>T p.(Arg757*)] also

11 expected to undergo NMD. Family 3 included two sisters with global developmental impairment

12 identified as part of a large-scale study aiming to identify candidate new genetic causes of

13 disease.[32] Trio WES of DNA from the older sister (Family 3, II:2) identified a homozygous

14 canonical splice site variant Chr2(GRCh38):g.161964133A>C; NM_001178015:c.2863-2A>C, also

15 confirmed to be homozygous in her affected sibling. RT-PCR revealed that the variant resulted in

16 partial intron retention and a premature stop codon [r.(2772_2773ins2772+1_2772+175);

17 r.(2773_2781del)]; p.(Gln954_Phe955ins*13) expected to result in NMD (**Supplementary Fig.**

18 **3**). In Family 4, WES performed on DNA from two brothers, (Family 4, III:2 and III:3) identified

19 a shared homozygous *SLC4A10* nonsense variant in exon 20/27 expected to result in NMD

20 [Chr2(GRCh38):g.161957066G>A NM_001178015.1:c.2619G>A p.(Trp873*)]. In Family 5,

21 WES performed on DNA from two siblings and their parents identified a shared homozygous

22 *SLC4A10* haplotype comprising two missense variants, Chr2(GRCh38):g.161904888A>T

23 NM_001178015:c.1730A>T p.(Lys577Met) and Chr2(GRCh38):g.161976840A>T

24 NM_001178015:c.3308A>T; p.(Asn1103Ile), hereafter referred to as p.(Lys577Met;Asn1103Ile).

25 p.(Lys577Met) affects an invariantly conserved residue within a helical transmembrane domain

26 and is predicted deleterious by *in silico* tools Polyphen2 and SIFT with a high REVEL score

27 (0.873), whereas p.(Asn1103Ile) affects a highly conserved residue but is predicted deleterious

28 only by SIFT and benign by Polyphen with a low REVEL score (0.239) (**Table S2**). All the

29 *SLC4A10* variants identified in this study are absent from the Genome Aggregation Database

1 (gnomAD v2.1.1 and v3.1.2); furthermore, there are no homozygous loss-of-function variants in

2 canonical *SLC4A10* transcripts listed in publicly accessible genomic databases.

Clinical features of *SLC4A10*-related neurodevelopmental disorder

4 All ten affected individuals presented with hypotonia in infancy, with resultant significant feeding

5 difficulties in 4/10. Psychomotor development was delayed in all individuals across all domains

6 and intellectual impairment was typically severe. Affected individuals were non-verbal, with one

7 exception; although 7/10 children were ambulatory, walking was delayed in these children until

8 between 2-7 years of age. There was no evidence of developmental regression and while hearing

9 loss was noted in a *Slc4a10*^{-/-} mouse model,[23] it was not reported in any of the affected patients in

10 this study. Seizures were reported in three individuals, but in two cases these were isolated

11 episodes occurring in the first few years of life. In addition, an affected child from Family 4

12 displayed bitemporal epileptogenic discharges on EEG at age 5 years in the absence of overt

13 clinical seizures, with spontaneous resolution thereafter.

14 Behavioral abnormalities were very commonly present and included features associated with

15 autistic spectrum disorder such as anxiety and stereotyped movements (hand flapping, head

16 nodding), hyperactivity and in some cases aggressive episodes. OFC was reported to be normal at

17 birth, but recent measurements were below average in all cases (-1.7 SDS to -5.6 SDS) with 7/10

18 affected individuals meeting the criteria for microcephaly (<-3 SDS). Affected individuals were

19 below average weight for their age, with height relatively preserved.

20 Magnetic resonance imaging (MRI) neuroimaging findings were striking and consistent.

21 Neuroradiological features of the *SLC4A10*-related neurodevelopmental disorder included

22 microcephaly, with a relative preservation of brain volume compared to occipito-frontal

23 circumference and narrow sometimes slit-like lateral ventricles similar to those seen in the

24 *Slc4a10*^{-/-} mouse model (**Supplementary Fig. 4**), even in those cases with less well-preserved

25 cerebral volume. The corpus callosum was either normal, or dysmorphic (slightly thickened and

26 blunted, flattened in a cranio-caudal direction and with sharply descending fornix) (**Fig. 2,**

27 **Supplementary Fig. 5**). This is likely to be as a result of the small lateral ventricles displacing the

28 fornix and septum pellucidum. There was an absence of cortical malformations and myelination

29 was appropriate for age.

Recovery from acidification is delayed in cells expressing disease-associated SLC4A10 variants

We previously showed that acid extrusion is compromised in hippocampal neurons in acute brain slices from knockout mice.[22] Here, we sought to provide insight into the functional consequences of the SLC4A10 missense variants using cellular studies. We first cloned wild-type and variant *SLC4A10* cDNAs into the mammalian expression vector pBI-CMV4. Two days post-transfection into the fast-growing mouse neuroblastoma cell line N2a, cells were fixed with 4% PFA and stained with an antibody directed against an N-terminal epitope of SLC4A10 as described previously and with the lectin wheat germ agglutinin (WGA) to label glycan structures associated with the plasma membrane.[22,40] As expected, cells transfected with the wild-type *SLC4A10* construct displayed a predominant labelling at the plasma membrane, whereas the SLC4A10 p.(Lys577Met;Asn1103Ile) variant protein showed a predominant intracellular localization (**Supplementary Fig. 6A**). The quantification of signal intensities for the interior of cells (not including the WGA labelled surface) as compared to the plasma membrane region (the WGA labelled surface) allowed us to calculate the ratio between cell surface and intracellular intensities, which was significantly increased for the SLC4A10 p.(Lys577Met;Asn1103Ile) variant protein (**Supplementary Fig. 6B**).

While this outcome alone may explain the pathogenic mechanism of the SLC4A10 p.(Lys577Met;Asn1103Ile) variant, we also assessed the impact on transport activity by BCECF fluorescence imaging in transfected N2a cells in bicarbonate-buffered salt solution with or without 5 μM EIPA to block Na^+/H^+ exchange. Representative single cell traces are shown in **Supplementary Fig. 7A**. Compared with untransfected cells, steady state pH_i was slightly more alkaline in cells transfected with the *SLC4A10* wild-type construct (**Supplementary Fig. 7B**). A shift in pH_i remained for both the p.(Lys577Met) and the p.(Asn1103Ile) variant proteins but was present to a lesser extent for the combined p.(Lys577Met;Asn1103Ile) variant (**Supplementary Fig. 7C**). Bath application of 20 mM sodium propionate for 5 min induced an acid shift, the amplitude of which did not differ between wild-type and mutant constructs (**Supplementary Fig. 7D**). pH_i recovery during the propionate exposure was significantly faster for the wild-type construct compared to untransfected cells (transfected cells 163.1±22.9 %, untransfected cells 100.0±18.7%, n=7/7, bootstrap paired t-test p=0.001, **Supplementary Fig. 7E**). For

1   p.(Lys577Met), p.(Asn1103Ile) and p.(Lys577Met;Asn1103Ile) the alkaline overshoot after

2   propionate removal (which provides a quantification of net removal of acid during the propionate

3   exposure) was significantly smaller compared to wild type [bootstrap F-test p<0.001, post-hoc

4   tests: WT 287.5±18.2%, p.(Lys577Met) 169.2±14.0%, n=7/10, bootstrap t-test p<0.001, WT

5   287.5±18.2%, p.(Asn1103Ile) 231.8±24.9%, n=7/9, bootstrap t-test p<0.05, WT 287.5±18.2%,

6   p.(Lys577Met;Asn1103Ile) 139.6±18.6%, n=7/8, bootstrap t-test p<0.001] (**Supplementary Fig.**

7   **7F**). Taken together, we conclude that acid extrusion is significantly diminished in cells expressing

8   SLC4A10 p.(Lys577Met) and p.(Asn1103Ile) variants alone and p.(Lys577Met;Asn1103Ile) *in*

9   *cis*.

10

11 Slc4a10^{-/-} mice show behavioral abnormalities in the 2-object novel

12 object recognition task and display grossly intact cortical structure

13   The identification of biallelic *SLC4A10* variants in affected individuals with cognitive impairment

14   and behaviors associated with autistic spectrum disorders prompted us to reanalyze the behavior

15   of *Slc4a10^{-/-}* mice. In our previous paper, we reported that motor functions including activity,

16   locomotion and motor coordination, were not altered in *Slc4a10* knockout mice.[22] Here, we used

17   the 2-object novel object recognition (NOR) task to assess recognition memory, which is based on

18   the spontaneous tendency of rodents to spend more time exploring a novel object than a familiar

19   one.[41] Interestingly, *Slc4a10* knockout mice clearly displayed a marked avoidance of the novel

20   object (**Fig. 3A**).

21   As structural brain abnormalities were present in some of the affected patients, we also re-analyzed

22   the brain structure of *Slc4a10^{-/-}* mice. Overall, the brain was found to be smaller and the weight

23   reduced in knockout mice compared to wild type animals (**Fig. 3B**). As previously reported,[22] we

24   also noted smaller brain ventricles in *Slc4a10^{-/-}* mice, while the corpus callosum appeared intact

25   (**Fig. 3C, Supplementary Fig. 4**).

26   To test whether *Slc4a10^{-/-}* mice display abnormalities in cortex organization, we also counted

27   neurons labelled for the pan-neuronal marker NeuN (RBFOX3)[42] in sagittal sections of the motor

28   and the somatosensory cortex of 2-month-old adult mice. Overall, the number of neurons per layer

1　did not differ between genotypes (**Fig. 3D**), suggesting an absence of any gross cortical layering

2　defect in *Slc4a10*^{-/-} mice.

3

SLC4A10 modulates GABAergic but not glutamatergic transmission

6　To gain further insight regarding the role of SLC4A10 in neuronal functions, we co-stained mouse

7　brain sections for SLC4A10 and either VGLUT1 (**Fig. 4A**), a presynaptic marker of excitatory

8　synapses, or VGAT (**Fig. 4B**), a presynaptic marker of inhibitory synapses. We have previously

9　published control staining on knockout tissues.[22] Whereas the relative area of co-localization was

10　$6.4\pm0.5\%$ (n=28) for VGLUT1, it was $74.9\pm1.3\%$ (n=39) for VGAT (**Fig. 4C**). Pearson correlation

11　coefficients (CC) between SLC4A10 and either VGLUT1 or VGAT signals after the Costes

12　method[34] are in agreement with a predominant localization of SLC4A10 with GABAergic but not

13　glutamatergic presynapses (**Fig. 4C**, CC VGLUT1/SLC4A10 [0.03] versus CC VGAT/SLC4A10

14　[0.5], 28 and 39 images each).

15　These data led us to next study whether neurotransmitter release is affected in the CA1 region of

16　the hippocampus *Slc4a10*^{-/-} mice. Frequency, amplitude and kinetics of mEPSCs recorded in the

17　presence of TTX did not differ between genotypes (**Fig. 5A-C** and **Supplementary Table 4**)

18　suggesting that glutamate release is not affected by disruption of SLC4A10. In contrast, the

19　frequency of mIPSCs in TTX, either recorded in CA1 (**Fig. 5D-F**, **Supplementary Table 4**) or

20　CA3 (**Supplementary Fig. 8**), were significantly decreased in the presence of HCO_3^-. While

21　amplitudes were unaffected, τ_{decay} and consequently the transferred electric charge per event were

22　diminished in slices obtained from *Slc4a10*^{-/-} mice. As there is evidence that spontaneous and

23　evoked neurotransmission are partially segregated at inhibitory synapses,[43] we also studied

24　spontaneous postsynaptic currents (sIPSCs), the frequencies and kinetics of which were reduced

25　(**Supplementary Fig. 9**).

26　As the disruption of the acid-extruder SLC4A10 is expected to decrease neuronal pH_i,[22] we tested

27　whether the mIPSC frequency can be rescued by raising pH_i. Indeed, 20 mM trimethyl ammonium

28　(TriMA), which raises pH_i without affecting pH_o,[44] increased the mIPSC frequency in preparations

29　from *Slc4a10*^{-/-} mice (**Fig. 5D-F**), while the kinetics were not affected. Analogously, lowering pH_i

by replacing 20 mM NaCl by sodium propionate decreased mIPSC frequency in slices from wild-type mice (**Supplementary Fig. 10**). The effects of the disruption of *Slc4a10* on frequency and kinetics were eliminated under bicarbonate-free conditions in recordings performed in HEPES-buffered solution, arguing against structural defects or an altered subunit composition of postsynaptic GABA$_A$ receptors (**Fig. 5G**).

Together, these data show that SLC4A10 modulates GABAergic synaptic transmission in a HCO$_3^-$ dependent manner.

Discussion

Here we present clinical and genetic data from five unrelated families, alongside molecular and neurobiological findings in mice that define biallelic loss-of-function variants in *SLC4A10* as a cause of a severe neurodevelopmental disorder, frequently associated with microcephaly (<-3SDS) and morphologically abnormal collapsed (slit) lateral ventricles. This slit-like appearance of the lateral ventricles appears to be characteristic of the disorder and mirrors findings in the *Slc4a10$^{-/-}$* mouse.[22] SLC4A10 mediates Na$^+$-dependent acid extrusion at the basolateral side of choroid plexus epithelial cells.[22] Thus, collapsed brain ventricles in knockout mice and in patients with *SLC4A10* biallelic loss-of-function alleles suggest that basolateral SLC4A10-dependent Na$^+$ uptake plays a key role for the apical Na$^+$-coupled secretion of the cerebrospinal fluid (CSF).[45]

The four truncating *SLC4A10* variants identified are predicted to result in complete molecular loss of function [deletion of exons 5-11; p.(Trp140Argfs*39), p.(Arg757*), p.(Trp873*) and c.2863-2A>C; p.(Gln954_Phe955ins*13)]. Consistent with this, affected individuals homozygous for these variants have the most severe neurological outcomes. Additionally, while both the p.(Lys577Met), affecting the transmembrane region (**Supplementary Fig. 11**), and C-terminal p.(Asn1103Ile) variant proteins were each trafficked to the proximity of the plasma membrane individually, SLC4A10 protein harboring both p.(Lys577Met;Asn1103Ile) variants *in cis* was largely trapped intracellularly and acid extrusion was shown to be significantly diminished (**Supplementary Fig. 6A,E,F**), strongly supportive of pathogenicity.

Previously a *de novo* balanced translocation disrupting *SLC4A10* was identified as a candidate cause of disease in a single individual described to have "mental retardation, progressive cognitive

decline, and partial complex epilepsy".[26] However, a heterozygous *SLC4A10* variant causing a severe monogenic disease is not consistent with the autosomal recessive condition described here, given the unaffected parental / sibling carriers of loss-of-function *SLC4A10* variants, and the many heterozygous loss-of-function gene variants listed in gnomAD. While it remains unclear whether an undetected *SLC4A10* variant may have been present *in trans* with the disrupted *SLC4A10* allele, heterozygous loss of SLC4A10 function due to the translocation event alone appears unlikely to be responsible for the neurological condition affecting this individual.

Our findings are also of note in light of recent genome-wide association studies (GWAS) which identify a highly statistically significant association between *SLC4A10* intronic or in *cis* regulatory-transcription binding region variants and neurological traits including cognitive function, educational attainment, brain and hippocampal volume and psychiatric morbidity (**Supplementary Table 5**).[46-48] Taken together with our present findings, these data provide compelling evidence for the importance of *SLC4A10* in normal neurological development and function and suggest a potential role for *SLC4A10* in traits mediated by oligo/polygenic inheritance.

Notably, *Slc4a10*^{-/-} mice show altered object discrimination with avoidance of the novel object thus resembling a mouse model of autistic spectrum disorder.[49] This prompted us to use our mouse model to further characterize the role of SLC4A10 in brain function. We previously showed that SLC4A10 is broadly expressed in both principal cells and inhibitory interneurons and that its disruption impaired the recovery of neurons from an acid load in the somatodendritic compartment.[22] Here, we show that SLC4A10 co-localizes with a marker of GABAergic but not glutamatergic presynapses. In agreement with this localization, GABA release was reduced, while glutamate release was not affected. This defect is characterized by a decrease of mIPSC frequency, while mIPSCs amplitudes remain unaltered. Intracellular alkalinization with TriMA partially rescued mIPSC frequency in brain slices from *Slc4a10*^{-/-} mice, while intracellular acidification induced a decrease of mIPSC frequency in wild-type mice, which further supports the conclusion that the difference in mIPSC frequency between the two genotypes are pH_i dependent. The knockout of a plasma membrane resident Na^+-coupled anion exchanger such as SLC4A10 might also change the equilibrium potential for Na^+ (E_{Na}) excitability thus coupling E_{Na} to pH. It is conceivable that changes in E_{NA} lead to subtle changes in membrane potential. Such voltage

1 fluctuations can propagate along axons and thus modulate the amplitude of axonal action potentials

2 and postsynaptic potentials evoked by these spikes.[50] However, cellular Na^+ loading by pH-

3 regulatory mechanisms typically requires blocking the Na-K ATPase.[51] Moreover, the relative

4 permeability for Na^+ of a typical neuron at rest is very low compared to K^+ and Cl^- and thus exerts

5 only a minor contribution to the resting membrane potential.[52] In agreement, the resting membrane

6 potential between wild-type and knockout principal neurons did not differ at steady state, thus

7 excluding a major effect of SLC4A10 on E_{Na} and excitability of principal neurons. A limitation of

8 the current study is that we have been unable to study the basic electrophysiological properties of

9 interneurons. However, given that the basic properties of principal neurons are largely unaffected

10 by the disruption, it is highly likely that this also applies to interneurons.

11 In contrast to the decreased mIPSC frequency, mIPSC kinetics were only mildly changed, which

12 can reflect alterations at the postsynaptic site such as changes in the receptor density or the

13 composition of the receptor subunits.[53] However, the differences between genotypes were

14 abolished under bicarbonate-free conditions which eliminates the activity of Na^+-dependent HCO_3^-

15 transporters arguing against this possibility. Because GABA$_A$ receptor function critically depends

16 on extracellular pH,[4,54,55] changes in the kinetics rather suggest an increase in the pH of the synaptic

17 cleft. Accordingly, TriMA, which only raises pH_i, but does not affect extracellular pH,[56] did not

18 change mIPSC kinetics. Notably, the disruption of the Na^+/H^+ exchanger NHE1/SLC9A1, another

19 transporter expressed at inhibitory presynapses, also decreased mIPSC frequency and altered

20 kinetics.[11]

21 Thus, both SLC4A10 and SLC9A1 seem likely to contribute to the regulation of pH_i at GABAergic

22 nerve endings and, notably, biallelic variants in *SLC9A1* have been linked to a syndromic

23 neurological disorder.[57] Furthermore, control of pH_i at glutamatergic presynapses is mediated by

24 the combination of SLC9A1[11] and SLC4A8,[58] another Na^+-dependent HCO_3^- transporter closely

25 related to SLC4A10. Similar to the defect of GABA release upon disruption of SLC4A10,

26 disruption of SLC4A8 affects glutamate release via its effect on presynaptic pH_i. These data show

27 that changes in pH_i may affect the vesicle release machinery in both GABAergic and glutamatergic

28 neurons in numerous ways. Presynaptic Ca^{2+} transients, which trigger synaptic vesicle

29 exocytosis,[59] may be altered upon disruption of either *Slc4a8*, *Slc4a10* or *Slc9a1*, potentially

30 because both Ca^{2+} influx via voltage-gated Ca^{2+} channels (VDCCs)[2,60,61] and Ca^{2+} release from

intracellular stores[62,63] are strongly pH-dependent. Alternatively, H^+ may compete with Ca^{2+} at the binding site of synaptic vesicles, or may alter the function of proteins involved in vesicle release.[64] Changes in pHi might also affect the loading of GABA into synaptic vesicles, because VGAT operates as a GABA/H^+ exchanger and critically depends on the H^+ electrochemical gradient generated by the vacuolar-type H^+.[65,66] However, the lack of effect of disruption of SLC4A10 on mIPSC amplitudes are evidence against such an effect.[67]

Consistent with a defect of GABA release, we previously reported an increased network excitability in acute brain slices obtained from *Slc4a10* knockout mice as evidenced by compromised paired-pulse facilitation and increased excitatory postsynaptic potential-spike coupling (E-S coupling).[24] Changes in the production and composition of the CSF of *Slc4a10* knockout mice may have opposite effects on network excitability *in vivo*. Indeed, seizure susceptibility to pentylenetetrazole (PTZ) and hyperthermia-induced hyperventilation with respiratory alkalosis were diminished in *Slc4a10* knockout mice.[22] Whether patients with *SLC4A10*-related disease are at increased risk of developing seizures is as of yet unclear, and in our study only 2 out of 10 patients had a clear history of epilepsy

Patients with *SLC4A10* loss-of-function not only suffer from intellectual disability and behavioral abnormalities, but also show microcephaly and characteristic slit-like brain ventricles. Both the strong expression of SLC4A10 in choroid plexus epithelial cells and[21,22] the collapsed brain ventricles characteristic of this disease, are indicative of a severely reduced production of cerebrospinal fluid in patients. Historically the cerebrospinal fluid was primarily considered to provide a simple supportive environment for the brain. However, it is now appreciated that the cerebrospinal fluid is an integral component of the central nervous system with dynamic and diverse roles which commence during early brain development, for example maintaining the stemness of embryonic progenitor cells which contact the cerebrospinal fluid via their apical surface.[68] Moreover, explants cultured as neurospheres depend on age-matched cerebrospinal fluid in order to maintain appropriate progenitor identity, proliferation, and neuronal differentiation.[69,70] While our analyses did not identify gross alterations of the cortical structure in *Slc4a10* knockout mice, additional studies will be required to rule out more subtle structural changes. As cerebrospinal fluid components exchange with the interstitial fluid of the brain parenchyma, changes in cerebrospinal fluid production and composition may influence periventricular brain

structures such as the hippocampus and hypothalamus, but also potentially other brain structures that exchange with the interstitial fluid.[71] To identify potential consequences on synaptic functions, in the future it would be beneficial to generate and compare phenotypes of mice with a disruption of SLC4A10 either specifically in neurons, or in the choroid plexus.

In summary, we present extensive genetic, clinical, functional and murine datasets that confirm that biallelic *SLC4A10* pathogenic loss-of-function gene variants cause a syndromic neurodevelopmental disorder. Defects of GABAergic function are a recurrent finding in various neurodevelopmental and neuropsychiatric phenotypes such as intellectual disability, autistic spectrum disorders, epilepsy and schizophrenia.[72,73] Importantly, positive modulation of GABA$_A$ receptors by diazepam and GABA$_A$ receptor agonists have been shown to improve behavioral and neurophysiological defects in mouse models of fragile X syndrome.[74,75] Given this, it is tempting to hypothesize that enhancing inhibitory GABAergic transmission could be a possible therapeutic approach for ameliorating some of the neurological symptoms in patients with *SLC4A10*-related neurodevelopmental disorder.

Acknowledgements

Funding

Competing interests

The authors declare that there are no competing interests.

Supplementary material

Supplementary material is available at *Brain* online.

References

1. Traynelis SF, Cull-Candy SG. Proton inhibition of N-methyl-D-aspartate receptors in cerebellar neurons. *Nature*. May 24 1990;345(6273):347-50. doi:10.1038/345347a0

2. Tombaugh GC, Somjen GG. Effects of extracellular pH on voltage-gated Na+, K+ and Ca2+ currents in isolated rat CA1 neurons. *J Physiol*. Jun 15 1996;493 (Pt 3)(Pt 3):719-32. doi:10.1113/jphysiol.1996.sp021417

3. Waldmann R, Champigny G, Bassilana F, Heurteaux C, Lazdunski M. A proton-gated cation channel involved in acid-sensing. *Nature*. 1997/03/01 1997;386(6621):173-177. doi:10.1038/386173a0

4. Pasternack M, Smirnov S, Kaila K. Proton modulation of functionally distinct GABAA receptors in acutely isolated pyramidal neurons of rat hippocampus. *Neuropharmacology*. 1996;35(9-10):1279-88. doi:10.1016/s0028-3908(96)00075-5

5. Sinning A, Hübner CA. Minireview: pH and synaptic transmission. *FEBS Lett*. Jun 27 2013;587(13):1923-8. doi:10.1016/j.febslet.2013.04.045

6. Chesler M. Regulation and modulation of pH in the brain. *Physiol Rev*. Oct 2003;83(4):1183-221. doi:10.1152/physrev.00010.2003

7. Ruffin VA, Salameh AI, Boron WF, Parker MD. Intracellular pH regulation by acid-base transporters in mammalian neurons. *Front Physiol*. 2014;5:43. doi:10.3389/fphys.2014.00043

8. Sinning A, Liebmann L, Kougioumtzes A, Westermann M, Bruehl C, Hubner CA. Synaptic glutamate release is modulated by the Na+ -driven Cl-/HCO(3)(-) exchanger Slc4a8. *The Journal*

of neuroscience : the official journal of the Society for Neuroscience. May 18 2011;31(20):7300-11. doi:10.1523/JNEUROSCI.0269-11.2011

9.   Burette AC, Weinberg RJ, Sassani P, Abuladze N, Kao L, Kurtz I. The sodium-driven chloride/bicarbonate exchanger in presynaptic terminals. *J Comp Neurol*. May 1 2012;520(7):1481-92. doi:10.1002/cne.22806

10.   Salameh AI, Hübner CA, Boron WF. Role of Cl(-) -HCO(3)(-) exchanger AE3 in intracellular pH homeostasis in cultured murine hippocampal neurons, and in crosstalk to adjacent astrocytes. *J Physiol*. Jan 1 2017;595(1):93-124. doi:10.1113/jp272470

11.   Bocker HT, Heinrich T, Liebmann L*, et al*. The Na+/H+ Exchanger Nhe1 Modulates Network Excitability via GABA Release. *Cereb Cortex*. Sep 13 2019;29(10):4263-4276. doi:10.1093/cercor/bhy308

12.   Stawarski M, Hernandez RX, Feghhi T*, et al*. Neuronal Glutamatergic Synaptic Clefts Alkalinize Rather Than Acidify during Neurotransmission. *The Journal of Neuroscience*. 2020;40(8):1611-1624. doi:10.1523/jneurosci.1774-19.2020

13.   Feghhi T, Hernandez RX, Stawarski M*, et al*. Computational modeling predicts ephemeral acidic microdomains in the glutamatergic synaptic cleft. *Biophysical Journal*. 2021/12/21/ 2021;120(24):5575-5591. doi:https://doi.org/10.1016/j.bpj.2021.11.011

14.   Orlowski J, Grinstein S. Na+/H+ exchangers. *Compr Physiol*. Oct 2011;1(4):2083-100. doi:10.1002/cphy.c110020

15.   Romero MF, Chen AP, Parker MD, Boron WF. The SLC4 family of bicarbonate (HCO_3^-) transporters. *Mol Aspects Med*. Apr-Jun 2013;34(2-3):159-82. doi:10.1016/j.mam.2012.10.008

16.   Alper SL, Sharma AK. The SLC26 gene family of anion transporters and channels. *Mol Aspects Med*. Apr-Jun 2013;34(2-3):494-515. doi:10.1016/j.mam.2012.07.009

17.   Wang J, Wang W, Wang H, Tuo B. Physiological and Pathological Functions of SLC26A6. *Front Med (Lausanne)*. 2020;7:618256. doi:10.3389/fmed.2020.618256

18.   McMurtrie HL, Cleary HJ, Alvarez BV*, et al*. The bicarbonate transport metabolon. *J Enzyme Inhib Med Chem*. Jun 2004;19(3):231-6. doi:10.1080/14756360410001704443

19.   Damkier HH, Aalkjaer C, Praetorius J. Na+-dependent HCO3- import by the slc4a10 gene product involves Cl- export. *J Biol Chem*. Aug 27 2010;285(35):26998-7007. doi:10.1074/jbc.M110.108712

20. Parker MD, Musa-Aziz R, Rojas JD, Choi I, Daly CM, Boron WF. Characterization of human SLC4A10 as an electroneutral Na/HCO3 cotransporter (NBCn2) with Cl- self-exchange activity. *J Biol Chem*. May 9 2008;283(19):12777-88. doi:10.1074/jbc.M707829200

21. Praetorius J, Nejsum LN, Nielsen S. A SCL4A10 gene product maps selectively to the basolateral plasma membrane of choroid plexus epithelial cells. *Am J Physiol Cell Physiol*. Mar 2004;286(3):C601-10. doi:10.1152/ajpcell.00240.2003

22. Jacobs S, Ruusuvuori E, Sipilä ST, *et al*. Mice with targeted Slc4a10 gene disruption have small brain ventricles and show reduced neuronal excitability. *Proc Natl Acad Sci U S A*. Jan 8 2008;105(1):311-6. doi:10.1073/pnas.0705487105

23. Huebner AK, Maier H, Maul A, *et al*. Early Hearing Loss upon Disruption of Slc4a10 in C57BL/6 Mice. *J Assoc Res Otolaryngol*. Jun 2019;20(3):233-245. doi:10.1007/s10162-019-00719-1

24. Sinning A, Liebmann L, Hübner CA. Disruption of Slc4a10 augments neuronal excitability and modulates synaptic short-term plasticity. *Front Cell Neurosci*. 2015;9:223. doi:10.3389/fncel.2015.00223

25. Belengeanu V, Gamage TH, Farcas S, *et al*. A de novo 2.3 Mb deletion in 2q24.2q24.3 in a 20-month-old developmentally delayed girl. *Gene*. Apr 10 2014;539(1):168-72. doi:10.1016/j.gene.2014.01.060

26. Gurnett CA, Veile R, Zempel J, Blackburn L, Lovett M, Bowcock A. Disruption of sodium bicarbonate transporter SLC4A10 in a patient with complex partial epilepsy and mental retardation. *Archives of neurology*. Apr 2008;65(4):550-3. doi:10.1001/archneur.65.4.550

27. Krepischi AC, Knijnenburg J, Bertola DR, *et al*. Two distinct regions in 2q24.2-q24.3 associated with idiopathic epilepsy. *Epilepsia*. Dec 2010;51(12):2457-60. doi:10.1111/j.1528-1167.2010.02742.x

28. Sebat J, Lakshmi B, Malhotra D, *et al*. Strong association of de novo copy number mutations with autism. *Science*. Apr 20 2007;316(5823):445-9. doi:10.1126/science.1138659

29. Laver TW, De Franco E, Johnson MB, *et al*. SavvyCNV: Genome-wide CNV calling from off-target reads. *PLOS Computational Biology*. 2022;18(3):e1009940. doi:10.1371/journal.pcbi.1009940

30. Wagner M, Berutti R, Lorenz-Depiereux B*, et al*. Mitochondrial DNA mutation analysis from exome sequencing-A more holistic approach in diagnostics of suspected mitochondrial disease. *J Inherit Metab Dis*. Sep 2019;42(5):909-917. doi:10.1002/jimd.12109

31. Mayr JA, Haack TB, Graf E*, et al*. Lack of the mitochondrial protein acylglycerol kinase causes Sengers syndrome. *Am J Hum Genet*. Feb 10 2012;90(2):314-20. doi:10.1016/j.ajhg.2011.12.005

32. Monies D, Abouelhoda M, Assoum M*, et al*. Lessons Learned from Large-Scale, First-Tier Clinical Exome Sequencing in a Highly Consanguineous Population. *The American Journal of Human Genetics*. 2019/06/06/ 2019;104(6):1182-1201. doi:https://doi.org/10.1016/j.ajhg.2019.04.011

33. Novarino G, Fenstermaker AG, Zaki MS*, et al*. Exome sequencing links corticospinal motor neuron disease to common neurodegenerative disorders. *Science*. Jan 31 2014;343(6170):506-511. doi:10.1126/science.1247363

34. Dunn KW, Kamocka MM, McDonald JH. A practical guide to evaluating colocalization in biological microscopy. *American Journal of Physiology-Cell Physiology*. 2011;300(4):C723-C742. doi:10.1152/ajpcell.00462.2010

35. Liebmann L, Karst H, Sidiropoulou K*, et al*. Differential effects of corticosterone on the slow afterhyperpolarization in the basolateral amygdala and CA1 region: possible role of calcium channel subunits. *J Neurophysiol*. Feb 2008;99(2):958-68. doi:01137.2007 [pii]

10.1152/jn.01137.2007

36. Dwivedi AK, Mallawaarachchi I, Alvarado LA. Analysis of small sample size studies using nonparametric bootstrap test with pooled resampling method. S*tat Med.* Jun 30 2017;36(14):2187-2205. doi:10.1002/sim.7263

37. R*: A language and environment for statistical computing.* R Foundation for Statistical Computing; 2021. https://www.R-project.org/

38. R*Studio: Integrated Development Environment for R.* RStudio, PBC; 2021. http://www.rstudio.com/

39. g*ee: Generalized Estimation Equation Solver. R package version 4.13-23.* 2022. https://CRAN.R-project.org/package=gee

40. Chazotte B. Labeling membrane glycoproteins or glycolipids with fluorescent wheat germ agglutinin. C*old Spring Harb Protoc.* May 1 2011;2011(5):pdb.prot5623. doi:10.1101/pdb.prot5623

41. Grayson B, Idris NF, Neill JC. Atypical antipsychotics attenuate a sub-chronic PCP-induced cognitive deficit in the novel object recognition task in the rat. B*ehav Brain Res.* Nov 22 2007;184(1):31-8. doi:10.1016/j.bbr.2007.06.012

42. Munji RN, Choe Y, Li G, Siegenthaler JA, Pleasure SJ. Wnt signaling regulates neuronal differentiation of cortical intermediate progenitors. T*he Journal of neuroscience : the official journal of the Society for Neuroscience.* Feb 2 2011;31(5):1676-87. doi:10.1523/jneurosci.5404-10.2011

43. Horvath PM, Piazza MK, Monteggia LM, Kavalali ET. Spontaneous and evoked neurotransmission are partially segregated at inhibitory synapses. e*Life.* 2020/05/13 2020;9:e52852. doi:10.7554/eLife.52852

44. Eisner DA, Kenning NA, O'Neill SC, Pocock G, Richards CD, Valdeolmillos M. A novel method for absolute calibration of intracellular pH indicators. P*flugers Arch.* Mar 1989;413(5):553-8. doi:10.1007/bf00594188

45. Damkier HH, Brown PD, Praetorius J. Cerebrospinal fluid secretion by the choroid plexus. P*hysiol Rev.* Oct 2013;93(4):1847-92. doi:10.1152/physrev.00004.2013

46. Lee JJ, Wedow R, Okbay A, *et al.* Gene discovery and polygenic prediction from a genome-wide association study of educational attainment in 1.1 million individuals. N*ature genetics.* Jul 23 2018;50(8):1112-1121. doi:10.1038/s41588-018-0147-3

47. van der Meer D, Rokicki J, Kaufmann T, *et al.* Brain scans from 21,297 individuals reveal the genetic architecture of hippocampal subfield volumes. M*olecular psychiatry.* Nov 2020;25(11):3053-3065. doi:10.1038/s41380-018-0262-7

48. Ripke S, Neale BM, Corvin A, *et al.* Biological insights from 108 schizophrenia-associated genetic loci. N*ature.* 2014/07/01 2014;511(7510):421-427. doi:10.1038/nature13595

49. Kane MJ, Angoa-Peréz M, Briggs DI, *et al.* Mice genetically depleted of brain serotonin display social impairments, communication deficits and repetitive behaviors: possible relevance to autism. P*loS one.* 2012;7(11):e48975. doi:10.1371/journal.pone.0048975

50.   Shu Y, Hasenstaub A, Duque A, Yu Y, McCormick DA. Modulation of intracortical synaptic potentials by presynaptic somatic membrane potential. N*ature.* Jun 8 2006;441(7094):761-5. doi:10.1038/nature04720

51.   Kaila K, Voipio J. Postsynaptic fall in intracellular pH induced by GABA-activated bicarbonate conductance. N*ature.* Nov 12-18 1987;330(6144):163-5. doi:10.1038/330163a0

52.   Rutecki PA, Lebeda FJ, Johnston D. Epileptiform activity induced by changes in extracellular potassium in hippocampus. J*ournal of neurophysiology.* Nov 1985;54(5):1363-74. doi:10.1152/jn.1985.54.5.1363

53.   Farrant M, Kaila K. The cellular, molecular and ionic basis of GABA(A) receptor signalling. P*rog Brain Res.* 2007;160:59-87. doi:10.1016/s0079-6123(06)60005-8

54.   Dietrich CJ, Morad M. Synaptic acidification enhances GABAA signaling. T*he Journal of neuroscience : the official journal of the Society for Neuroscience.* Nov 24 2010;30(47):16044-52. doi:10.1523/jneurosci.6364-09.2010

55.   Mozrzymas JW, Żarnowska ED, Pytel M, Mercik K. Modulation of GABA$_A$ Receptors by Hydrogen Ions Reveals Synaptic GABA Transient and a Crucial Role of the Desensitization Process. T*he Journal of Neuroscience.* 2003;23(22):7981-7992. doi:10.1523/jneurosci.23-22-07981.2003

56.   Stenkamp K, Palva JM, Uusisaari M, *et al.* Enhanced temporal stability of cholinergic hippocampal gamma oscillations following respiratory alkalosis in vitro. J*ournal of neurophysiology.* May 2001;85(5):2063-9. doi:10.1152/jn.2001.85.5.2063

57.   Guissart C, Li X, Leheup B, *et al.* Mutation of SLC9A1, encoding the major Na^+/H^+ exchanger, causes ataxia-deafness Lichtenstein-Knorr syndrome. H*um Mol Genet.* Jan 15 2015;24(2):463-70. doi:10.1093/hmg/ddu461

58.   Grichtchenko, II, Choi I, Zhong X, Bray-Ward P, Russell JM, Boron WF. Cloning, characterization, and chromosomal mapping of a human electroneutral Na(+)-driven Cl-HCO3 exchanger. J *Biol Chem.* Mar 16 2001;276(11):8358-63. doi:10.1074/jbc.C000716200

59.   Schneggenburger R, Neher E. Intracellular calcium dependence of transmitter release rates at a fast central synapse. N*ature.* Aug 24 2000;406(6798):889-93. doi:10.1038/35022702

60.   Doering CJ, McRory JE. Effects of extracellular pH on neuronal calcium channel activation. N*euroscience.* May 25 2007;146(3):1032-43. doi:10.1016/j.neuroscience.2007.02.049

61. Fraire-Zamora JJ, González-Martínez MT. Effect of intracellular pH on depolarization-evoked calcium influx in human sperm. A*m J Physiol Cell Physiol.* Dec 2004;287(6):C1688-96. doi:10.1152/ajpcell.00141.2004

62. Tsukioka M, Iino M, Endo M. pH dependence of inositol 1,4,5-trisphosphate-induced Ca2+ release in permeabilized smooth muscle cells of the guinea-pig. J *Physiol.* Mar 15 1994;475(3):369-75. doi:10.1113/jphysiol.1994.sp020078

63. Ma J, Fill M, Knudson CM, Campbell KP, Coronado R. Ryanodine receptor of skeletal muscle is a gap junction-type channel. S*cience.* Oct 7 1988;242(4875):99-102. doi:10.1126/science.2459777

64. Rizo J, Xu J. The Synaptic Vesicle Release Machinery. A*nnual Review of Biophysics.* 2015;44(1):339-367. doi:10.1146/annurev-biophys-060414-034057

65. Farsi Z, Preobraschenski J, van den Bogaart G, Riedel D, Jahn R, Woehler A. Single-vesicle imaging reveals different transport mechanisms between glutamatergic and GABAergic vesicles. S*cience.* Feb 26 2016;351(6276):981-4. doi:10.1126/science.aad8142

66. Egashira Y, Takase M, Watanabe S, *et al.* Unique pH dynamics in GABAergic synaptic vesicles illuminates the mechanism and kinetics of GABA loading. P*roceedings of the National Academy of Sciences.* 2016;113(38):10702-10707. doi:doi:10.1073/pnas.1604527113

67. Frerking M, Borges S, Wilson M. Variation in GABA mini amplitude is the consequence of variation in transmitter concentration. N*euron.* 1995/10/01/ 1995;15(4):885-895. doi:https://doi.org/10.1016/0896-6273(95)90179-5

68. Paridaen JT, Wilsch-Bräuninger M, Huttner WB. Asymmetric inheritance of centrosome-associated primary cilium membrane directs ciliogenesis after cell division. C*ell.* Oct 10 2013;155(2):333-44. doi:10.1016/j.cell.2013.08.060

69. Chau Kevin F, Springel Mark W, Broadbelt Kevin G, *et al.* Progressive Differentiation and Instructive Capacities of Amniotic Fluid and Cerebrospinal Fluid Proteomes following Neural Tube Closure. D*evelopmental Cell.* 2015/12/21/ 2015;35(6):789-802. doi:https://doi.org/10.1016/j.devcel.2015.11.015

70. Lehtinen MK, Zappaterra MW, Chen X, *et al.* The cerebrospinal fluid provides a proliferative niche for neural progenitor cells. N*euron.* Mar 10 2011;69(5):893-905. doi:10.1016/j.neuron.2011.01.023

71. Fame RM, Lehtinen MK. Emergence and Developmental Roles of the Cerebrospinal Fluid System. D*ev Cell.* Feb 10 2020;52(3):261-275. doi:10.1016/j.devcel.2020.01.027

72. Levitt P, Eagleson KL, Powell EM. Regulation of neocortical interneuron development and the implications for neurodevelopmental disorders. T*rends Neurosci.* Jul 2004;27(7):400-6. doi:10.1016/j.tins.2004.05.008

73. Schmidt-Wilcke T, Fuchs E, Funke K, *et al.* GABA-from Inhibition to Cognition: Emerging Concepts. N*euroscientist.* Oct 2018;24(5):501-515. doi:10.1177/1073858417734530

74. Heulens I, D'Hulst C, Van Dam D, De Deyn PP, Kooy RF. Pharmacological treatment of fragile X syndrome with GABAergic drugs in a knockout mouse model. B*ehav Brain Res.* Apr 1 2012;229(1):244-9. doi:10.1016/j.bbr.2012.01.031

75. Olmos-Serrano JL, Corbin JG. Amygdala regulation of fear and emotionality in fragile X syndrome. D*ev Neurosci.* 2011;33(5):365-78. doi:10.1159/000329424

Figure legends

Figure 1 Family pedigrees and biallelic *SLC4A10* variants. A) Simplified family pedigrees for individuals affected with *SLC4A10*-related neurodevelopmental disorder, showing autosomal recessive segregation of *SLC4A10* variants. Co-segregation confirmed in other family members as indicated, in each case '+' indicating variant allele and '-' indicating wild type allele. **B)** Simplified *SLC4A10* exon structure (NM_001178015.2) showing location of the multi-exon deletion identified in Individuals III:1 and III:2 (Family 1) and the splicing variant (c.2863-2A>C). Only a part of the large, non-coding, UTR Exon 27 is shown. **C)** Simplified SLC4A10 protein structure (Q5DTL9-1) showing location of missense (yellow) and predicted loss-of-function (red) variants in relation to the predicted domain architecture (Pfam domains- https://www.ebi.ac.uk/interpro/) of SLC4A10. Cytoplasmic: Band 3 cytoplasmic domain (PF07565); HCO_3^- transporter: HCO_3^- transporter family (PF00955). **D)** Multi-species alignments of SLC4A10, showing each of the missense variants identified in this study. Abbreviations: aa = amino acids.

Figure 2 Neuroimaging from affected individuals with biallelic SLC4A10 variants. (A,E,J) Family 1, III:1.T2-weighted axial (**A**), T1-weighted sagittal (**E**) and T1-weighted coronal (**J**) Magnetic resonance (MR) images of the patient at age 5 years. **(B,F,K) Family 1, III:2** T2-weighted axial (**B**), T1-weighted sagittal (**F**) and T1-weighted coronal (**K**) MR images of the patient at age 4 years. **(C,G,L) Family 2, II:1**. T2-weighted axial (**C**), T2-weighted sagittal (**G**) and T2-weighted coronal (**L**) MR images of the patient at age 10 months. **(D,H,M) Family 3, II:1** T2-weighted axial (**D**), T1-weighted sagittal (**H**) and T2-weighted coronal (**M**) MR images at age 1 year 2 months. In all cases lateral ventricles are small (**A**-**D** – arrowhead) with normal 4th ventricle (**E**-**H**), posterior fossa and external cerebrospinal fluid (CSF) spaces. In Family 1 the corpus callosum is dysmorphic, appearing thickened and flattened (**E,F**). This is associated with an unusual configuration of the fornix and septum pellucidum especially in Family 1, III:1 (**E** - arrowhead). In Families 2 and 3 it is hypoplastic (**G,H**). Myelination is complete or adequate for age in all cases. Normal MRI brain images for comparison are available at https://www.imaios.com/en/e-Anatomy/Brain/Brain-MRI-in-axial-slices (adult) and https://radiopaedia.org/cases/normal-mri-head-3-years-old-1?lang=gb (three-year-old child).

Figure 3 *Slc4a10*^{-/-} mice show behavioral abnormalities in the 2-object novel object recognition task and display grossly intact cortical architecture. A) The recognition of the novel object is altered in knockout (KO) mice. Upper: Illustration of the 2-object novel object recognition (NOR) test. Lower: During the NOR test the exploration time, the number of visits for the old and the new, and the duration of these visits were quantified. A difference score (time exploring novel object - time exploring familiar object) and the discrimination ratio (time exploring the novel versus the familiar object) was calculated (9 mice per genotype, bootstrap t-test; * $p < 0.05$; ** $p < 0.01$, *** $p < 0.001$). **B)** Top view of dissected brains from 12-month-old *Slc4a10* wild-type (WT) and KO mouse. The weight of perfused and fixed brains of KO mice was smaller compared to WT (n=5 mice per genotype; bootstrap t-test; ** $p < 0.01$). Scale bar: 2 mm. **C)** The gross architecture of the somatosensory cortex appeared intact in *Slc4a10* KO mice. Sagittal brain sections from 2-month-old *Slc4a10* WT and KO mice were stained for the pan neuronal marker NeuN and neurons counted layer wise (n=3 mice per genotype; GEE model using

1 normal errors identity link and independent working correlation matrix). Scale bar: 75 µm.

2 Quantitative data are presented as mean + standard error of the mean (SEM).

3

4 **Figure 4 Localization of SLC4A10 to GABAergic presynapses.** *Slc4a10* wild-type (WT) mouse

5 brain sections (Scale bars: 20 µm, enhanced view of merged marker images also shown (boxed

6 areas). **A)** VGLUT1, a marker of excitatory presynaptic terminals, rarely co-localizes with

7 SLC4A10 in the CA1 region of the hippocampus (green: SLC4A10, red: VGLUT1). **B)** SLC4A10

8 and VGAT, a marker for GABAergic presynapses, co-localise in the CA1 region of the

9 hippocampus (green: SLC4A10, red: VGAT). **C)** Quantitative analysis of co-localization of

10 SLC4A10 with either VGLUT1 or VGAT and calculation of Pearson correlation coefficients

11 between these data in the CA1 region of the hippocampus (VGLUT1 n=28 and VGAT n=39

12 images each, bootstrap t-test; *** $p < 0.001$).

13

14 **Figure 5 SLC4A10 acts on presynaptic pH_i to promote GABA release in CA1 pyramidal**

15 **neurons. Glutamatergic transmission is not impaired in CA1 neurons of *Slc4a10*$^{-/-}$ mice (A-**

16 **C).** **A)** Representative miniature excitatory postsynaptic current (mEPSC) recordings pyramidal

17 neurons from *Slc4a10* wild-type (WT) and knockout (KO) mice. **B)** Averaged mEPSCs show that

18 the kinetics of mEPSCs are not affected by disruption of *Slc4a10*. **C)** Cumulative plots and bar

19 charts of different mEPSC properties. No significant differences were detected in mEPSC

20 frequency, amplitude or kinetics (n=9/14;bootstrap t-test; n.s. not significant). **(D-G)** The mIPSC

21 frequency is diminished in *Slc4a10*$^{-/-}$ mice in the presence of bicarbonate. **D)** Representative

22 recordings of ongoing miniature inhibitory postsynaptic current (mIPSC) activity in pyramidal

23 neurons from *Slc4a10* wild-type (WT) and knockout (KO) mice as well of pyramidal neurons from

24 *Slc4a10* KO mice in the presence of 20 mM trimethylamine chloride (TriMA). **E)** Averaged

25 mIPSC recordings of pyramidal neurons from *Slc4a10* WT and KO mice to illustrate kinetics and

26 amplitude. **F)** Cumulative plots and bar charts of mIPSC properties (n=12/19/11; bootstrap F-test

27 with post-hoc analysis: * p<0.05; **p<0.01; ***p<0.001; n.s.: not significant). While no

28 differences in the mean amplitudes of mIPSCs were observed, the frequency of mIPSCs was

29 significantly diminished in cells derived from *Slc4a10* KO mice but could be partially rescued by

30 application of TriMA. Diminished τ_{decay} and half-width of averaged mIPSCs in pyramidal neurons

from *Slc4a10* KO mice compared with WT in bicarbonate-buffered artificial cerebrospinal fluid were not affected by TriMA. **G)** In HEPES-buffered nominally bicarbonate-free solution mIPSC frequencies and kinetics did not differ between genotypes (n=14/12; bootstrap t-test: * $p<0.05$; **$p<0.01$; ***$p<0.001$; n.s.: not significant). Quantitative data are shown as mean + standard error of the mean (SEM).
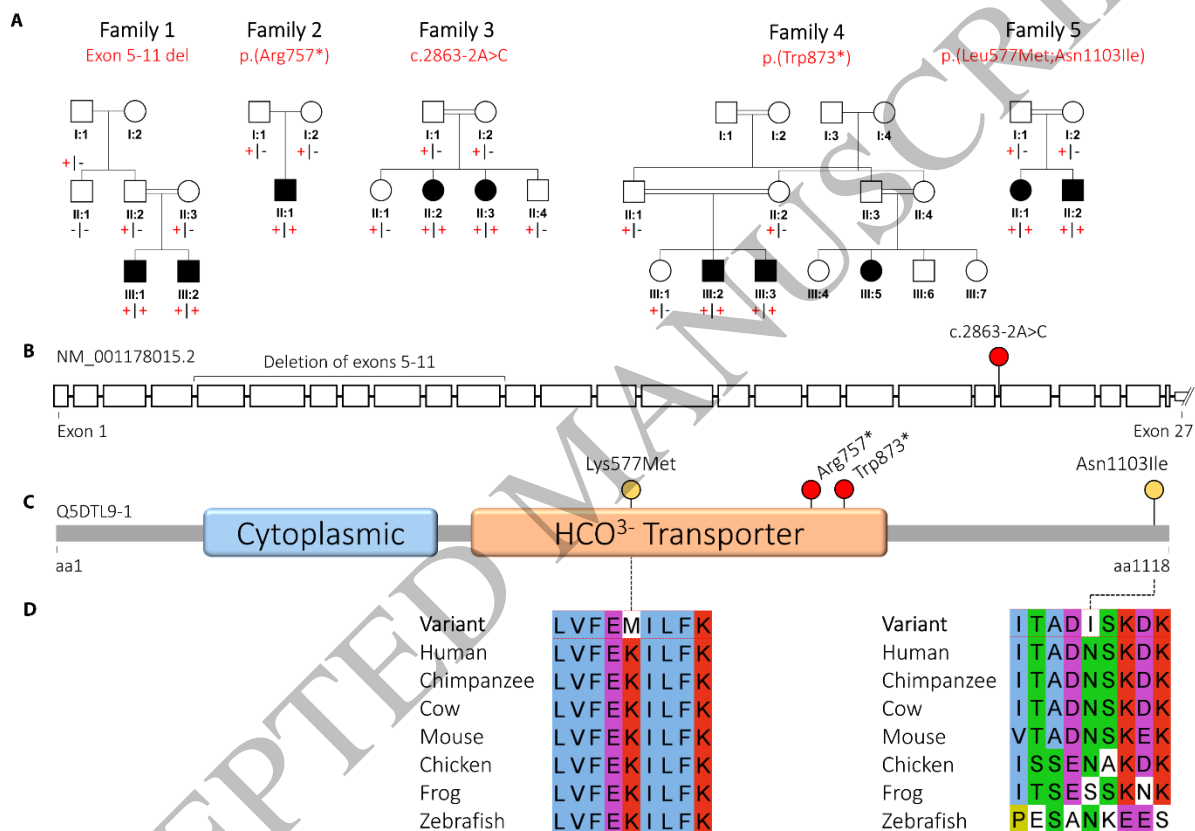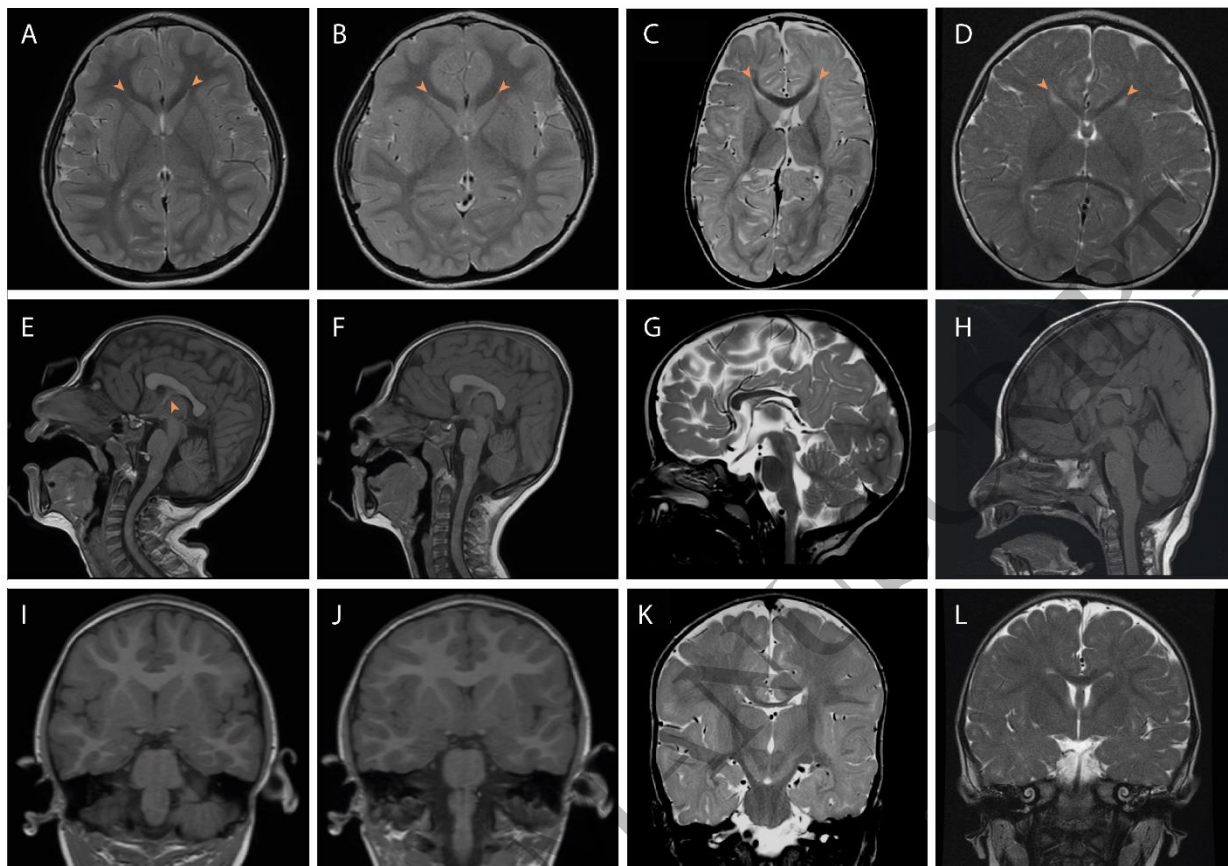

Figure 1
270x185 mm (x DPI)
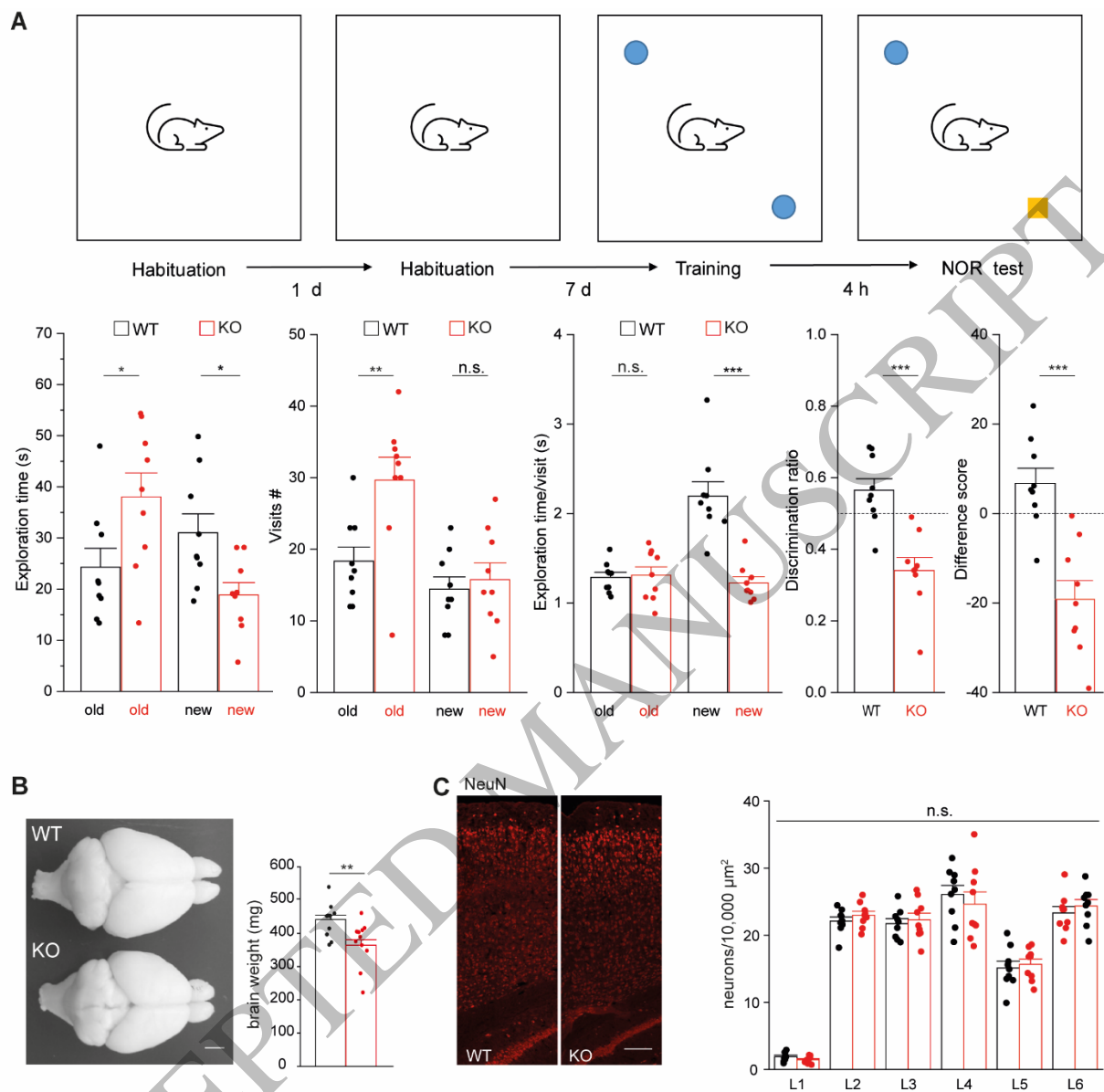
1

2 *Figure 2*
3 *294x207 mm (x DPI)*

1

2

3

4

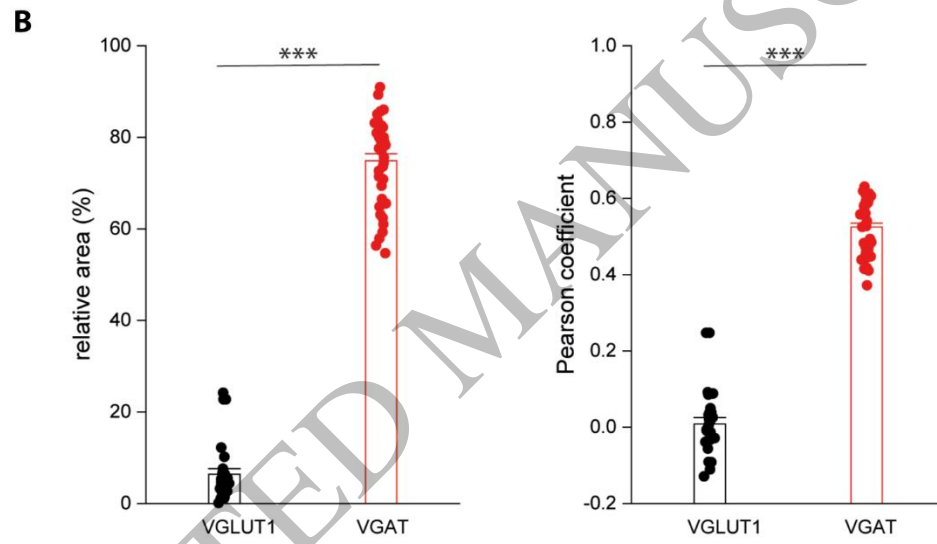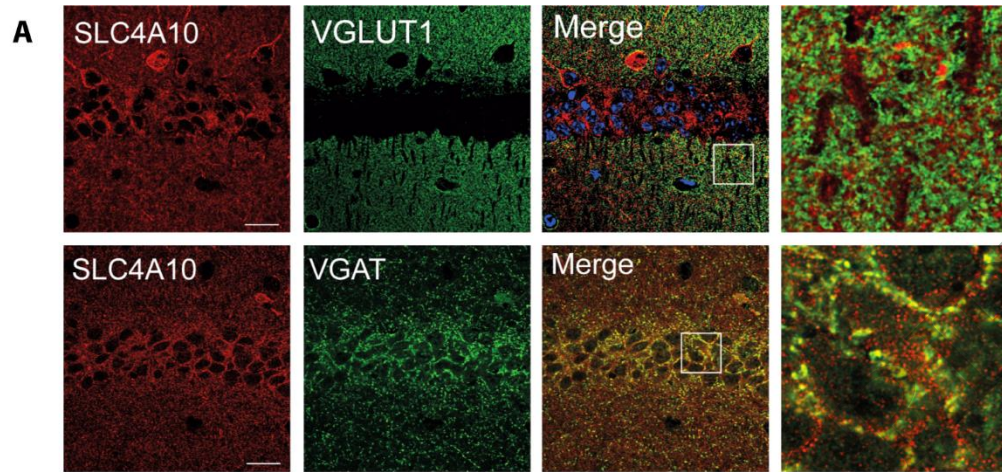*Figure 3*
193x187 mm (x DPI)

1
2
3
4

Figure 4
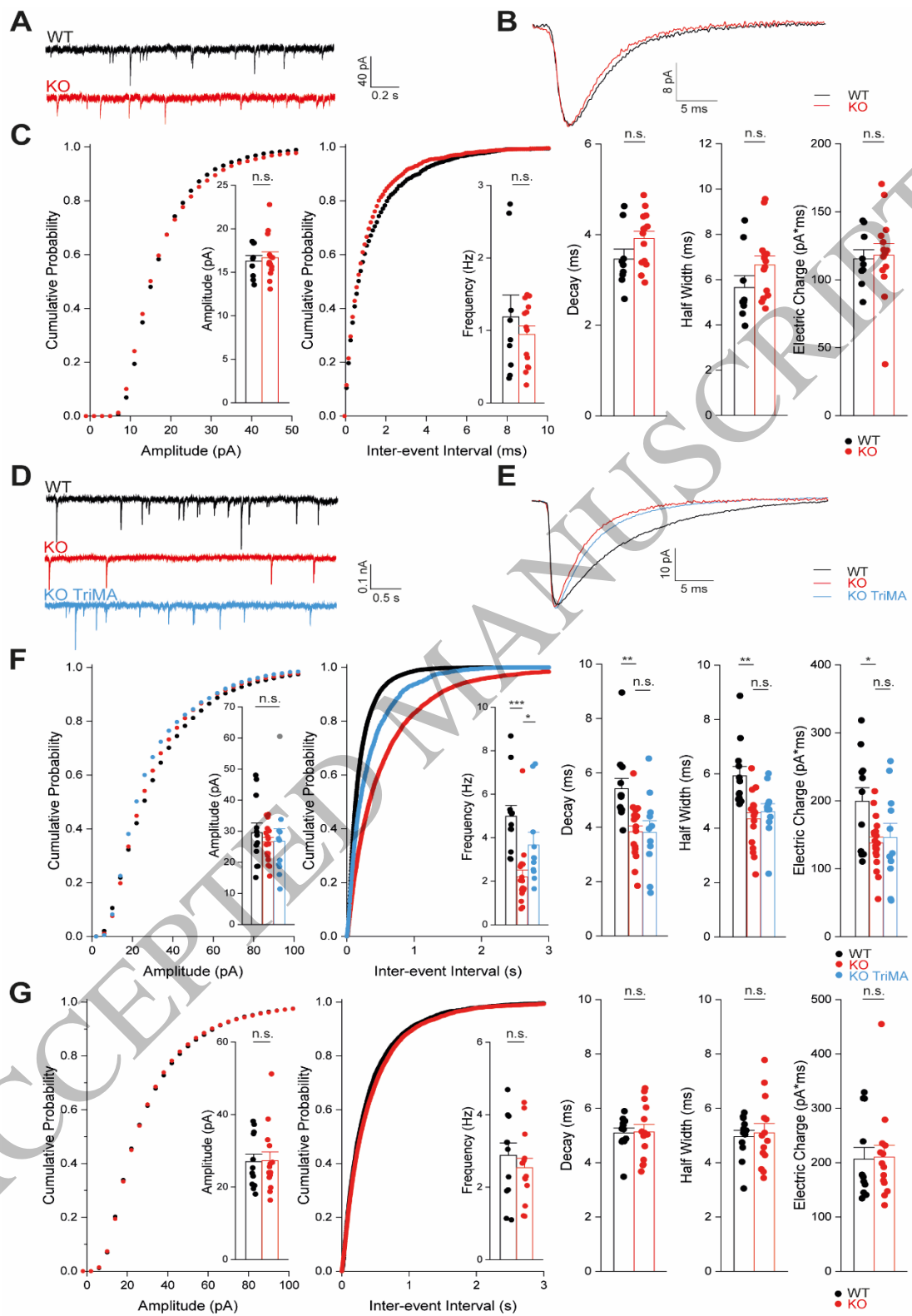*135x141 mm (x DPI)*

1

2   *Figure 5*
3   *191x296 mm (x DPI)*

Table 1 Clinical findings in individuals with biallelic *SLC4A10* variants

Individual	Family 1 III:1	Family 1 III:2	Family 2 II:1	Family 3 II:2	Family 3 II:3	Family 4 III:2	Family 4 III:3	Family 4 III:5	Family 5 II:1	Family 5 II:2
NM_001178015	Homozygous deletion of exons 5–11	Homozygous deletion of exons 5–11	Homozygous p.(Arg757*)	Homozygous c.2863-2A>C p.(Gln954_Phe955ins*13)	Homozygous c.2863-2A>C p.(Gln954_Phe955ins*13)	Homozygous p.(Trp873*)	Homozygous p.(Trp854*)	Homozygous p.(Trp854*)	Homozygous p.(Lys577Met; Asn1103Ile)	Homozygous p.(Lys577Met; Asn1103Ile)
Sex, age	M, 8 y 10 m	M, 7 y 8 m	M, 4 y 8 m	F, 8 y	F, 4 y	M, 10 y	M, 6 y 3 m	F, 17 y 5 m	F, 11 y	M, 6 y
Ethnicity	Palestinian	Palestinian	European	Arab Saudi	Arab Saudi	Egyptian	Egyptian	Egyptian	Turkish	Turkish
Birth OFC	NK	NK	NK	Normal	NK	34.2 [−0.8]	35 [−0.2]	33[−13]	NK	NK
OFC, cm [SDS]	50.5 [−2.3]	48.5 [−3.4]	50 [−1.7]	47.5 [−4.5]	44.5 [−5.5]	45.5 [−5.6]	46.6 [−4.3]	48 [−5.4]	51.6 [−1.9]	46.7 [−4.2]
Height, cm [SDS]	NK	NK	101.5 [−1.3]	125 [−0.4]	100 [−0.4]	123 [−2.5]	104 [−2.7]	150 [−2.2]	136 [−1.2]	111 [−1.0]
Weight, kg [SDS]	NK	NK	10.7 [−4.9]	19.8 [−1.8]	10.9 [−3.5]	23 [−2.3]	16 [−2.5]	45 [−1.8]	30.4 [−0.9]	17 [−1.7]
Feeding difficulties	NK	NK	Yes	Yes At birth	NK	No	No	Yes	Yes	Yes
Neuro/development										
Intellectual disability	Yes, severe	Yes, severe	Yes, severe	Yes, severe	Yes, severe	Yes, severe	Yes, severe	Yes, severe	Yes, moderate	Yes, severe
Gross motor	Walked >2 y	Walked 5 y	Rolling	Crawling	Not rolling	Walked 6 y	Walked 6 y	Walked 7 y	Walked 2 y	Walked 3 y
Speech	Non-verbal	Non-verbal	Babbles	Babbles	Sounds	Non-verbal	Non-verbal	Non-verbal	Dysarthria	Non-verbal
Hearing loss	No	No	No	NK	NK	No	No	No	No	No
Anxiety	Yes	Yes	No	Yes	No	Yes	Yes	Yes	No	Yes
Stereotypies	No	Yes	No	Yes	No	Yes	Yes	Yes	No	No
Hyperactivity	Yes	Yes	No	No	No	Yes	Yes	Yes	No	No
Seizures	Yes	Yes ?	No	Yes GTCS	No	Abn. EEG	No	No	No	No
Central tone	↓	↓	↓	↓	↓	↓	↓	↓	↓	↓
Peripheral tone	↑	↑	↓	↑	↓	↓	↓	↓	↓	↑
Tendon reflexes	+++	+++	++	+++ and clonus	NK	++	++	++	++	+++
MRI brain										
Slit lateral ventricles	Yes	Yes	Yes	NK	Yes	NK	NK	NK	Yes	Yes
Dysmorphic CC	Yes	Yes	Yes	NK	Yes	NK	NK	NK	No	Yes
Fornix/SP	Yes	Yes	Yes/No	NK	Yes	NK	NK	NK	No	Yes
Other findings										
Other					Craniosynostosis					

Yes = feature is present; No = feature is absent; +++ = exaggerated or brisk; ++ = normal; downwards arrow = decreased; upwards arrow = increased; Abn. EEG = abnormal electroencephalogram; F = female; Fornix/SP = distorted configuration of fornix / septum pellucidum; GTCS = generalized tonic-clonic seizures; M = male; m = months; NK = not known; OFC = occipitofrontal circumference; SDS = standard deviation scores from the mean; y = years.